Int. J. Electrochem. Sci., 11 **(2016)** 154 - 164

International Journal of
ELECTROCHEMICAL
SCIENCE
www.electrochemsci.org

High Reversible Silicon/Graphene Nanocomposite Anode for Lithium-Ion Batteries

Changjing Fu[*], *Chunlai Song, Lilai Liu, Weiling Zhao, Xuedong Xie*

School of Materials Science and Engineering, Heilongjiang University of Science and Technology, Harbin 150022, P.R. China
[*]E-mail: fcj_hit@163.com

Received: 19 October 2015 / *Accepted:* 11 November 2015 / *Published:* 1 December 2015

Si/graphene nanocomposites have been successfully synthesized by the in-situ growth and magnesium thermal reduction method. The composition and structure of the composite were characterized by the X-ray diffraction (XRD), Raman spectrum, X-ray photoelectron spectroscopy (XPS) and transmission electron microscopy (TEM), respectively. Electrochemical properties were evaluated in two-electrode cells versus metallic lithium. Results showed that Si nanoparticles, c.a. 10 nm in diameter, uniformly distributed within the graphene matrix forming a perfect conducting network. Galvanostatic charge-discharge cycling of the Si/graphene composite anode exhibited a reversible discharge capacity of more than 592 mAh g^{-1} after 500 cycles at the current density of 2 A g^{-1}, and 429 mAh g^{-1} at 8 A g^{-1}. Even after 80 cycles at various rates from 0.5 to 8 A g^{-1}, it still maintained the specific capacity of 892 mAh g^{-1} at 0.5 A g^{-1}. The excellent cycle performance and rate capability ensured that it might be applied to the high-power lithium-ion batteries as a flexible, high capability and conductivity anode.

Keywords: Silicon; graphene; composite; anode; lithium-ion batteries

1. INTRODUCTION

With the rapid depletion of fossil resources, the problems of the global energy crisis, environmental pollution and climate abnormality become more and more serious [1]. As one of the most efficient environmentally friendly energy storage systems, rechargeable lithium-ion batteries (LIBs) have attracted much attention in the social and industrial fields [2,3]. They have been widely used in portable electronics and are considered to be promising candidates to satisfy the demanding requirements of powering electric vehicles due to their excellent energy conversion efficiencies and relatively high energy densities [4]. However, in view of the limited theoretical capacity of the

commercial graphite anode materials (372 mAh/g), much effort has been devoted to develop new electrode materials with high energy and power densities [5,6].

Silicon based materials have been regarded as one of the most promising anode materials for the next generation LIBs since they offer a lower working potential, the highest known theoretical charge capacity and the abundant resources on earth [7]. Unfortunately, the structure damage by the volume change of silicon (>300%) and the continuous interfacial reaction caused by the electrolyte remains to the major challenges restricting their applications [8]. In addition, the lower electrical conductivity of silicon anode depresses the capability of the charge and discharge rate and the power output efficiency of LIBs. Many studies have been devoted to the resolution of the problems and demonstrated that reducing the size of silicon particles and fabrication of silicon-based composite materials with special structures are the most effective ways to achieve the improved cycle performance [9-12].

Recently, there is much attention focusing on the composites of Si and carbon materials with high electrical conductivity and small volume changes on lithiation, such as Si-carbon nanotubes and Si- graphene sheets [13, 14]. Although graphene has a high lithium ion storage capacity because of its special 2D structure, the graphene electrode shows a poor stability for the restacking of graphene [15]. As a novel carbon based material, however, graphene appears to be an attractive matrix to disperse Si nanoparticles due to its high electric conductivity, mechanical strength and flexibility [16-18]. In this case, graphene sheets play key roles in serving both as an electrically conductive network and an elastic buffer for the Si particles [19-21]. Si-graphene materials seem to have alleviated the issues associated with the bare Si and graphene [22]. However, it remains a challenge to evenly disperse Si within the graphene sheets. Thus, it is difficult to form a stable composite and lithium ion diffusion is hindered by the sluggish ion diffusion within the poorly distributed composite materials [23, 24].

Therefore, downsizing from bulk to various nanoscales morphologies/structures and dispersing these nanostructured Si into carbon matrix are the most appealing approaches being pursued to solve these issues and to enhance the electrochemical performance of the anodes containing Si in rechargeable LIBs [25, 26]. Here a low-cost and high-yield fabrication method was developed to in situ synthesis Si nanoparticles/graphene composites for high-performance LIBs. In order to avoid the demanding synthetic conditions, complicated procedure or micro-scale yield, magnesiothermic reduction of SiO_2 was chosen because of its potential for low-cost large-scale production. Moreover, graphene oxide was reduced at the same time. Under the optimized conditions, Si nanoparticles uniformly deposited on the thermal reduced graphene oxide sheets, forming ordered sandwich-structured Si/graphene nanocomposites.

2. EXPERIMENTAL

2.1 Preparation of Si/graphene composites

Graphene oxide (GO) was prepared by the modified Hummers method as we reported previously [33]. The final suspension of GO is controlled at 8 mg mL^{-1}. Thus-obtained GO suspension

(60 mL) was firstly diluted to 200 mL with deionized water, followed by adding 100 mL ethonal and 5 mL ammonium hydroxide. At the same time, tetraethyl orthosilicate (TEOS, 10 mL) was added into 100 mL ethanol while stirring. The TEOS suspension was then added into the GO suspension in drops. After stirring continuously for 5 h, the mixture was left to age for 12 h at room temperature. Thus-prepared sample was washed with deionized water and ethanol for several times until the pH value of the filtered solution is 7, and then freeze-dried overnight. After that, the dried sample was evenly mixed with magnesium powders. The weight ratio of the dried sample to magnesium powder is controlled at 0.8:1. The heat-treatment of the mixture was carried out in a laboratory tube furnace at 650 ^{o}C for 4 h in N_2. Next, the reduced powders soaked in 1 M HCl for 2 days to remove MgO. The black mixture was collected by centrifugation. After repeated washing with deionic water and ethanol, the Si/graphene composite was finally obtained by freeze-drying.

2.2 Characterization of Si/graphene composites

The XRD pattern of the as-prepared Si/graphene powder was obtained on Rigaku MinFlex, D/max 2550-PC X-ray diffractometer with Cu Ka radiation (λ=0.15406 nm). The scattering angles (2θ) were between 10^{o} and 80^{o} and the scanning rate was 5^{o} min^{-1}. Transmission electron microscopy (TEM) and high-resolution TEM (HRTEM) observations were conducted on a JEOL-2100F transmission electron microscope operated at 200 kV. Scanning transmission electron microscopy (STEM) measurement was performed on the JEOL JEM-2100F transmission electron microscope equipped with a Thermo Fisher Scientific energy-dispersed X-ray spectrometer. The dispersion of the sample was dripping on the carbon-coated TEM grid and air-dried. In order to obtain the surface chemistries characteristics of the materials, X-ray photoelectron spectroscopy (XPS) analysis was carried out on an AXIS Ultra instrument from Kratos Analytical in the range of 1-1300 eV. Raman spectra were recorded on a WITec CRM200 confocal Raman spectrometer with a 514.5 nm laser and a 2 μm spot. Thermogravimetry/differential scanning calorimetry (TG/DSC) was carried out on a Netzsch STA449C from room temperature to 800^{o}C at a heating rate of 10^{o}C min^{-1} in air.

2.3 Electrochemical measurements of Si/graphene composites anode

The electrochemical performance of the Si/graphene composite electrode was carried out using CR2025 coin-cells. The active materials, conductive carbon black, and polyvinylidene fluoride (PVDF) were mixed together in a weight ratio of 8:1:1. Thus-prepared mixture was further diluted by N-methyl pyrrolidinone (NMP) to form slurry, which was then spread onto the copper foil by a doctor-blade. The electrode film was dried under vacuum at 80^{o}C for 8 h. Cells were assembled inside an argon-filled glovebox. Lithium metal foils were taken as the counter electrode and the reference electrode, and the micro-porous polypropylene as the electrolyte membrane. The electrolyte was 1 M $LiPF_6$ solution dissolved in a mixture of EC and DMC (1:1 in volume ratio). The assembled cells were laid aside for one day before the electrochemical test. Cyclic Voltammery was examined with a CHI660C electrochemical workstation between 0.01 V and 3 V at a scanning rate of 0.1 mV s^{-1}.

Electrochemical impedance spectroscopy (EIS) tests were carried out on a M2273 electrochemical workstation. The frequency was controlled in the range of 10 mHz - 100 kHz. Galvanostatic charge and discharge cycles were tested by a NEWARE battery tester between 0.01 and 3.0 V (vs. Li^+/Li). All the electrochemical tests were performed at room temperature (25±1 ^oC).

3. RESULTS AND DISCUSSION

3.1. Structure and morphology of Si/graphene composites

The crystal structure of the synthesized product was analyzed by the recording XRD peaks of the final material.

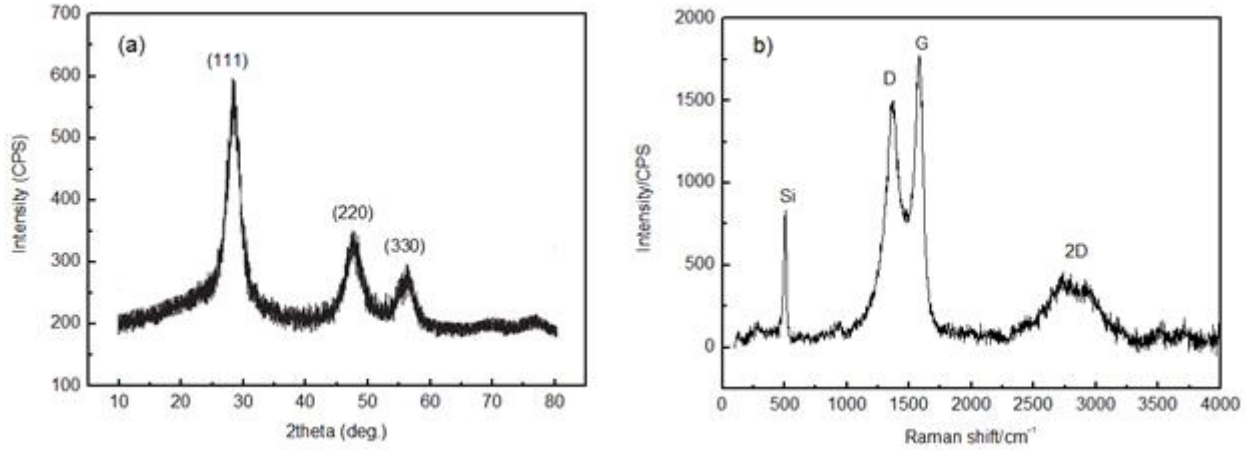

Figure 1. (**a**) XRD pattern of Si/graphene nanocomposite; (**b**) Raman spectrum of Si/graphene nanocomposite.

Fig.1a shows the XRD pattern of the sample. The diffraction pattern of the composite is in good agreement with the cubic Si (JCPDS card No. 27-1402). The diffraction peaks at $2\theta=28.4^o$, 47.3 and 56.1^o can be attributed to the Si (111), (220) and (311) structure, respectively. The characteristic diffraction peak of graphite at 26.4^o didn't appear, revealing that Si nanoparticles deposited on the graphene surface could efficiently suppress the stacking of reduced graphene layers, thus, in this case, no graphite-like layered structure formed again [28]. Fig.1b shows the Raman spectra of Si/graphene nanocomposites. A main peak at about 507 cm^{-1} is corresponding to Si nanoparticles [29]. Three other peaks at approximately 1355 cm^{-1}, 1578 cm^{-1} and 2736 cm^{-1} are associated with the D band, G band and 2D band peaks of graphene, respectively [30]. The integral ratio of I_D/I_G for Si/graphene nanocomposite is 1.49, indicating a decrease in the average size and an increase in the number of the sp^2 graphite domain compared to the original reduce graphene oxides [27].

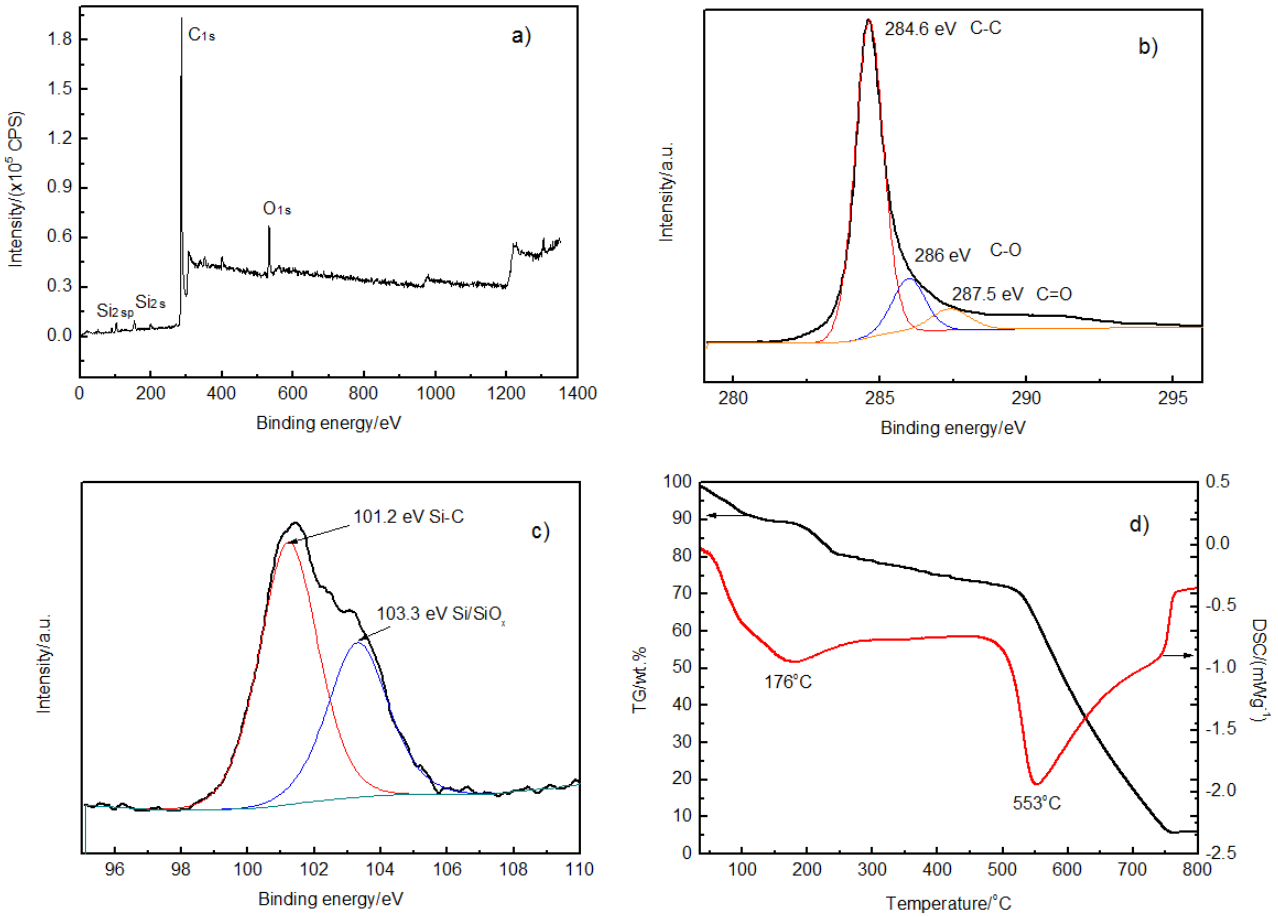

Figure 2. (**a**) General XPS spectrum of Si/graphene nanocomposite; (**b**) Low-resolution C1s XPS spectrum of Si/graphene nanocomposite; (**c**) Low-resolution Si2p XPS spectrum of Si/graphene nanocomposite; (**d**) TG/DSC curves of Si/graphene nanocomposite.

Important information on surface state and elemental compositions of the Si/graphene composites were studied by XPS, as shown in Fig.2. The elemental compositions obtained from the general spectrum (fig.2a) indicate that the atomic content of Si element was very low (4.03 at.%), which was lower than the result of TGA (fig.2d). This observation could be attributed to the fact that Si nanoparticles were covered by the reduced graphene oxide layers, giving the penetrating depth of the XPS being only one atomic layer or 5 nm. Figure 2b shows the XPS C1s spectrum of Si-graphene composites, the peak at 284.6, 286 and 287.5 eV is assigned to C=C/ C-C in the aromatic rings, C-O bond from the overlapping of C-O-C and C-OH (C-O of epoxy), and C=O groups, respectively. The high-resolution spectrum for Si2p is shown in fig.2c. The peak at 101.2 eV corresponds to the Si-C group and 103.3 eV corresponds to Si/SiO_x (x<2), suggesting a strong chemical bond existing between Si and graphene. Although there are no peaks of SiO_2, the SiO_x species are possibly by the oxidation of the freshly prepared Si nanoparticles, which are with high surface activity. As an intermediate phase connecting both Si and graphene, the formation of SiO_x thin layer could further enhance the adhesion between them. Figure 2d shows the TG/DSC curves of Si-graphene composite. There are two endothermic peaks in the DSC curve. The peak at 176^{o}C is attributed to the evaporation of the

absorbed water by the nanocomposite. The peak at 553^{o}C originates from the oxidation of a large amount of high activity graphene. The weight ratio of graphene in the composite was determined by the TG analysis. The infection point at approximately 523^{o}C in the TG curve separates the curve into two parts with different rates of mass loss. By combing these results with those from DSC curve, it can be seen that the part ranges from approximately 242 ~ 759 ^{o}C with a mass loss of 74% being attributed to the oxidation of graphene in the composite. Thus, the weight ratio of graphene in the composite is 74 wt.%, and the phases containing Si is approximately 26 wt.%.

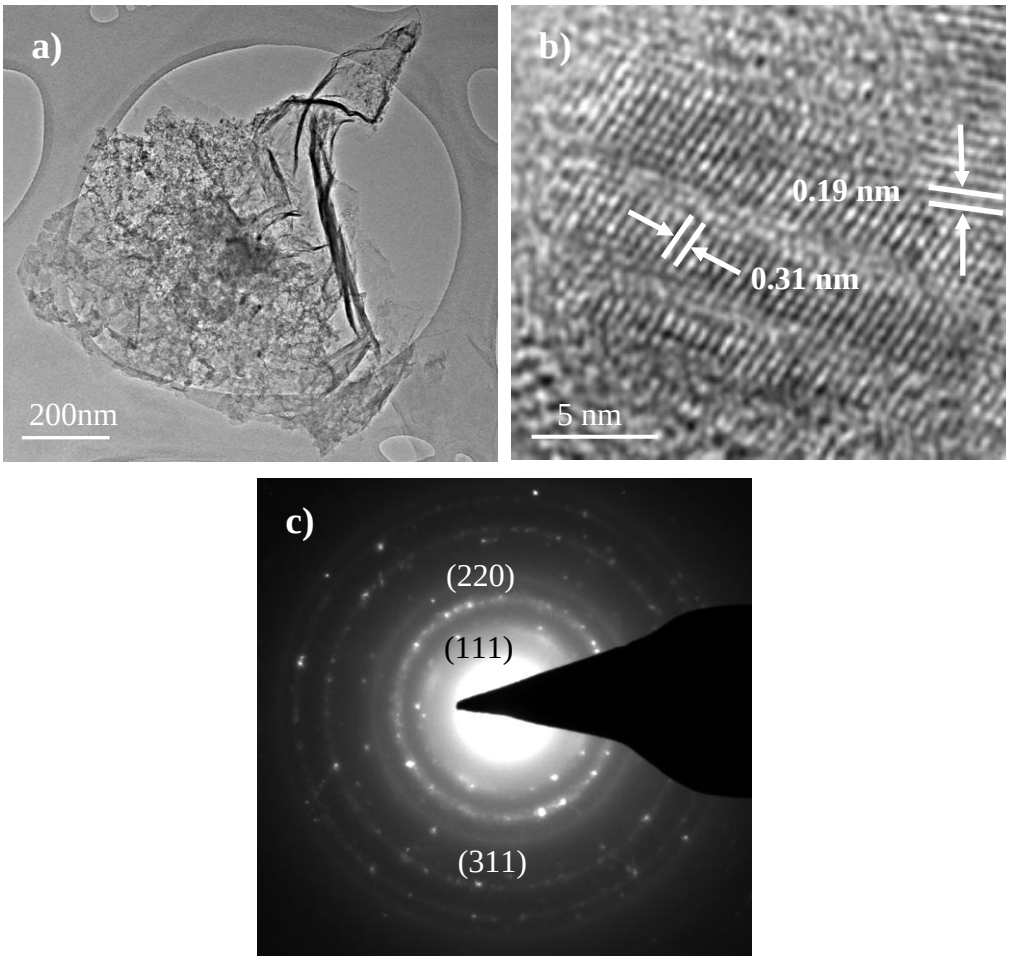

Figure 3. TEM images of Si/graphene nanocomposite: **(**a**)** Low-resolution and **(**b**)** High-resolution; (c) electron diffraction pattern.

Figure 3 shows the morphology and structure of the as-prepared Si/graphene composite. The low-magnification TEM image (fig.3a) reveals that the Si/graphene nanosheet still presents a flexible sheet-like appearance similar to that of graphene sheets. Although suffered from the high-temperature reduction reaction and acid washing, the sample still remains the sheet-like morphology and no agglomeration appeared. And Si nanoparticles disperse discretely on the surface of graphene. To characterize the internal structure of Si/graphene composite more precisely, we also investigated the sample using HRTEM. The highly magnified image presented in fig.3b reveals that the fringe spacing is 0.31 nm and 0.19 nm corresponding to the (111) and (220) plane of Si, respectively. A selected-area

electron diffraction pattern is shown in fig.3c and is well-indexed as a cubic Si phase (Si (111) (220) and (311)), which is consistent with the XRD results. The nanocrystals are in the diameters of less than 10 nm. The smaller of Si nanoparticles and the optimized microstructure of Si/graphene composite are expected to offer a better rate capability of the anode.

3.2 Electrochemical properties of Si/graphene composite anodes

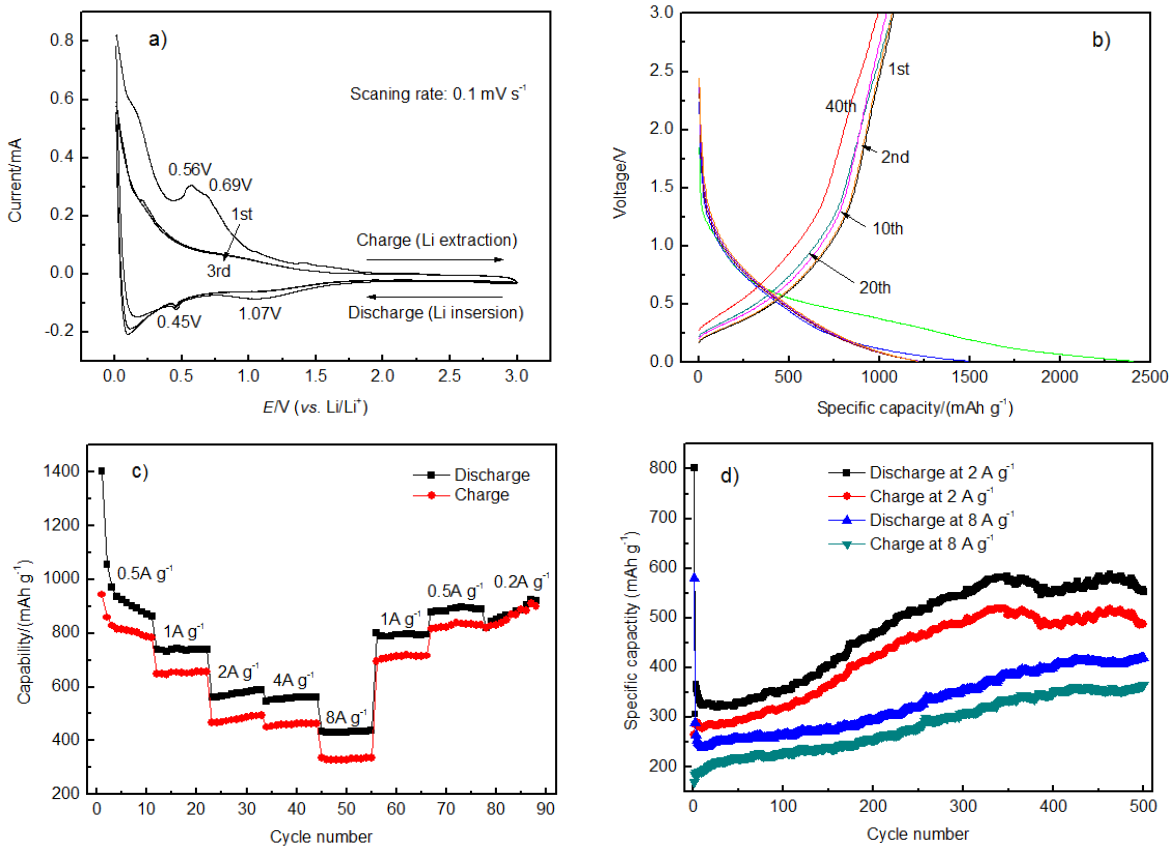

Figure 4. **(**a**)** Cyclic voltammograms curves of Si/graphene nanocomposite from 1st cycle to 3rd cycle at a scan rate of 0.1 mV s^{-1} in the voltage range of 0.01 to 3.0 V; **(**b**)** Galvanostatic discharge-charge profiles at 100 mA g^{-1}; **(**c**)** Rate capability at the current densities from 0.5 to 8 A g^{-1}; **(**d**)** Cycling performance of Si/graphene nanocomposite under 2 A g^{-1} and 8 A g^{-1}, respectively.

A series of electrochemical measurement were performed to study the Li-ion storage capabilities of the Si/graphene composite. Figure 4a shows the cyclic voltammetry (CV) curves of the first, second and third cycles of the Si/graphene nanocomposite at a scan rate of 0.1 mV s^{-1}. The observed redox peaks in the CV curves are in agreement with the previous report [30]. A discharge potential plateau appeared at c.a. 1.07 V during the first cathodic sweep, a reflection of the formation of a solid electrolyte interface (SEI) film and the possible irreversible Li ion insertion into the Si particles.

The plateau disappeared in the subsequent cycles suggesting the formation of stable SEI layers. The small peak at 0.45 V and the sharp peak at about 0.1 V resulted directly from the formation of Li-

Si alloys. In the anodic sweep, the peaks at 0.56 V and 0.69 V were assigned to the de-alloying of Li-Si alloys, which disappeared after several cycles. Besides that from the CV curves, we can also infer that for the Si/graphene composite anode, the capacity above 2 V (vs. Li/Li^+) contributes very few for the total capacity.

The charge-discharge voltage profiles of the Si/graphene electrode (fig.4b) were obtained for the first, second, tenth, twentieth and fortieth cycles at a current density of 100 mA g^{-1}. The potential plateaus observed in the discharge curves were consistent with the CV results, but it didn't have low potential flat plateaus as the conventional graphite anode. The insertion process gave a first discharge capacity of 2375 mAh g^{-1} and a charge capacity of 1081 mAh g^{-1}, resulting in a coulombic efficiency of 45.5%. The irreversible capacity losses in the first cycle were attributed to the decomposition of electrolyte forming a sold-electrolyte interface (SEI). Despite the large irreversible loss during the first cycle, a high discharge capacity of 1468 mAh g^{-1} was attained in the second cycle and the coulombic efficiency increased to 73% with a corresponding charge capacity of 1071.6 mAh g^{-1}. The coulombic efficiency further increased to 88% during the third charge-discharge cycle.

In addition to obtain the good capacity retention, Si/graphene nanocomposite electrodes also demonstrated an enhanced rate capability, as shown in fig.4c. With the increase in the current density, the Si/graphene electrode delivered a reversible capacity of 787.2, 663.5, 497.8, 466.8 and 343 mAh g^{-1} at the current density of 0.5, 1.0, 2.0, 4.0 and 8.0 A g^{-1}, respectively. A reversible capacity of 837.6 mAh g^{-1} was achieved after the rate changed back to 0.5 A g^{-1}. Moreover, this kind of nanocomposite electrodes presented an obviously enhanced capacity when the current density changed back from 8 A g^{-1} to 1 and 0.5 A g^{-1}. The specific capacity increased to 721.5 mAh g^{-1} at a current density of 1 A g^{-1}, increasing 8.7%, while at 0.5 A g^{-1}, it increased 5.9%, reaching 833.6 mAh g^{-1}. However, the specific capacity of the black Si electrode was only 664, 473, 389 and 353 mAh g^{-1}, at the current density of 1.0, 2.0, 3.0 and 4.0 mA g^{-1}, respectively [31]. The capacities of reduced graphene oxide (rGO) were 415, 342, 307, 166 mAh g^{-1}, at the current density of 200, 400, 800 and 4000 mA g^{-1}, respectively [32]. Compared with the black Si and rGO electrode, the good rate performance of the Si/graphene nanocomposites is attributed to the higher electrical conductivity and the special 2D structure of graphene, which would not only greatly reduce the intrinsic ohm resistance of the nanocomposite electrode, but also facile the Li ion diffusion.

Figure 4d shows the cycling performance of the Si/graphene nanocomposites. Two electrodes were cycled between 0.01 and 3.0 V at the current density of 2 A g^{-1} and 8 A g^{-1}, respectively. From this profile, we can see clearly that the discharge and charge capacities decrease slightly at the initial (approximately in the first 17 cycles) and then a significant increase in the specific capacity from the 17 th to 430 th cycle for the current density of 2 A g^{-1}, and from the 17 th to the 350 th cycle for the current density of 8 A g^{-1}, respectively. Then both of them tend to be steady with a slow increase. The highest discharge capacities are 592 and 429 mAh g^{-1} for the current density of 2 A g^{-1} and 8 A g^{-1}, respectively. The enhanced reversible capacity, excellent cyclic performance and rate capability highlight the advantages of this kind of Si/graphene nanocomposite. This phenomenon could be attributed to its special structure, the unique activation process of Si anode, as well as 3D porous graphene network [26]. For the Si anode, the activation phenomenon is due to the Li-Si alloying and dealloying process resulting in significant internal structural changes and the reconstruction of crystal

structure near the Si surface [33]. Moreover, graphene in this composite can not only provide a support for dispersing Si nanoparticles and work as a highly conductive matrix confirming a good contact between them, but can also effectively inhibit the volume expansion/contraction and aggregation of Si nanoparticles during the charge and discharge process [32]. Additionally, the bond interconnection (Si-C) between Si and graphene building a perfect conductive network leads to even smaller interparticles contact resistance and further accelerates the transport of Li^+ and electron in the anode [19].

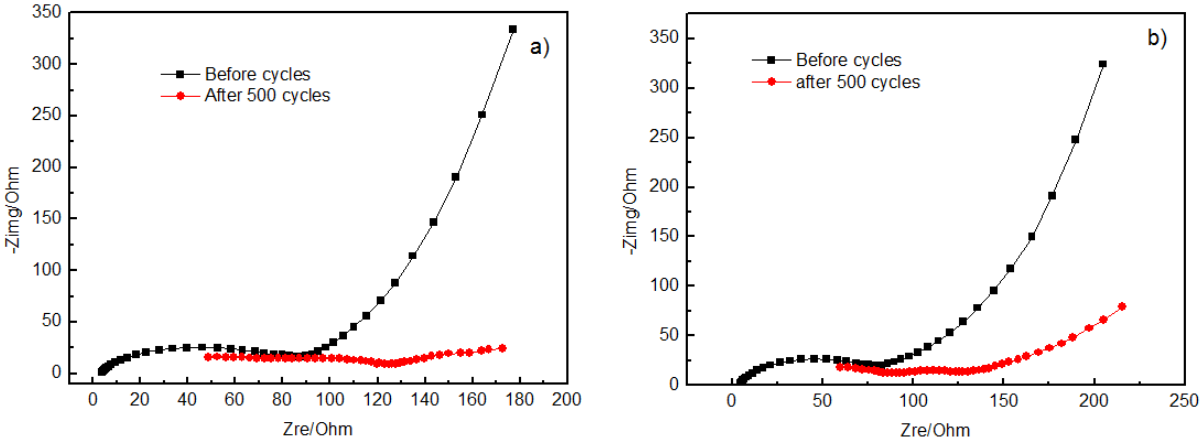

Figure 5. **(**a**)** Nyquist plots of Si/graphene nanocomposite under 2 A g^{-1}; **(**b**)** Nyquist plots of Si/graphene nanocomposite under 8 A g^{-1}.

In order to gain a better understanding of why Si/graphene nanocomposite exhibits a reduced discharge capacity after 500 cycles, EIS measurements were carried out as shown in fig.5. For the LIBs, the charge transfer kinetics and the rate of transfer reaction are determined by the charge transfer resistance and the charge-transfer process, respectively [15]. In the Nyquist plot, the diameter of the semicircle in the medium frequency range reflects the charge-transfer resistance (R_{ct}) occurring between active materials and liquid electrolyte. While the straight line is corresponding to the so-called Warburg diffusion, reflects the diffusion of lithium ions into electrode materials [28, 29]. For the sample cycled at the current density of 2 A g^{-1} (fig.5a), R_{ct} was 85.2 Ω before cycling and decreased to 76.6 Ω after 500 cycles (ΔR_{ct}=-8.7 Ω). The reduced R_{ct} indicates that the charge transfer kinetics changed very little revealing a relatively stable microstructure of the anode. ΔR_{ct} of the sample cycled at 8 A g^{-1} (fig.5b), was even lower, -8.45 Ω after 500 cycles. This was consistent with results of the cycle performance and rate capability, suggesting that Si/graphene anode had formed a good conductive network between Si nanoparticles and graphene, and the degradation of the charge transfer kinetics could be effectively suppressed. However, the Ohmic resistance (R_Ω) and the resistance for the Li^+ diffusion increased greatly for the both samples after 500 cycles, which may be the reason resulted in the reduced capacity. The postmortem study showed that a certain amount of the electrode had been stripped from the copper foil surface after 500 cycles, which further confirmed the EIS analysis.

4. CONCLUSIONS

The Si/graphene nanocomposite electrode prepared by the in situ magnesiothermic reduction method exhibited high power and energy densities simultaneously. Because of the special layered-sphere structure and high conductive pathways, the 3D Si/graphene nanocomposite presented the high gravimetric specific capacity, better cycling performance and excellent rate capability. The superior electrochemical performance of this material could be associated with its unique features, such as excellent electrical conductivity, short transportation path for both lithium-ions and electrons, elastomeric space to accommodate volume changes upon Li insertion/extraction and the strong connection between Si and graphene. But the increase in ohmic resistance and the Li^+ dispersion resistance resulted in the reduced discharge capacity since approximately the 500th cycle. Nevertheless, it is reasonable to consider that this kind of Si/graphene nanocomposite is a promising candidate as the anode of high-performance LIBs for electric vehicles.

ACKNOWLEDGEMENTS
This work was supported by Heilongjiang Provincial Natural Science Foundation (B201416).

References

1. D.F. He, F.J. Bai, L.X. Li, L.M. Shen, H.H. Kung and N.Z. Bao, *Electrochim. Acta*, 169 (2015) 409.
2. G. Jeong, Y. Kim, H. Kim and H. Sohn, *Energy Environ. Sci*., 4 (2011) 1986.
3. B. Scrosati and J. Garche, *J. Power Sources*, 195 (2010) 2419.
4. Z.-L. Xu, B. Zhang and J.-K. Kim, *Nano Energy*, 6 (2014) 27.
5. M. Winter and J.O. Besenhard, *Electrochim. Acta*, 45 (1999) 31.
6. M. Winter, J.O. Besenhard, M.E. Spahr and P. Novak, *Adv. Mater*., 10 (1998) 725.
7. N. Li, S.X. Jin, Q.Y. Liao, H. Cui and C.X. Wang, *Nano Energy*, 5 (2014) 105.
8. A. Magasinski, P. Dixon, B. Hertzberg, A. Kvit, J. Ayala and G. Yushin, *Nat. Mater*., 9 (2010) 353.
9. M.R. Zamfirm, H.T. Nguyen, E. Moyen, Y.H. Lee and D. Prinbat, *J. Mater. Chem. A*., 1 (2013) 9566.
10. H. Kim, M. Seo, M. Park and J. Cho, *Angew Chem*., 122 (2010) 2192.
11. R. Yi, F. Dai, M.L. Gordin, H. Sohn and D. Wang, *Adv. Energy Mater*., 3 (2013) 1507.
12. Y. Park, N. Choi, S. Park, S.H. Woo, S. Sim, B.Y. Jang, S.M. Oh, S. Park, J. Cho and K.T. Lee, *Adv. Energy Mater*., 3 (2013) 206.
13. S.H. Ng, J.I. Wang, D. Wexlar, K. Konstantinov, Z.P. Guo and H.K. Liu, *Angew. Chem. Int. Ed*., 45 (2006) 6896.
14. H. Kim and J. Cho, *Nano Lett*., 8 (2008) 3688.
15. J.T. Zai and X.F. Qian, *RCS Adv.*, 5 (2015) 8814.
16. Y. Shi, S.-L. Chou, J.-I. Wang, H.-J. Li, H.-K. Liu and Y.-P. Wu, *J. Power Sources*, 244 (2013) 684.
17. Y. Shi, J.I. Wang, S.L. Chou, D. Wexier and H.J. Li, *Nano Lett*., 13 (2013) 4715.
18. X. Wang, Q. Wang, X. Liu, X. Wang, D.M. Tang and W. Tian, *Nano Lett*., 14 (2014) 1164.
19. K.S. Novselov, A.K. Geim, S.V. Morozov, D. Jiang, Y. Zhang, S.V. Dubonos, I.V. Crigorieva and A.A. Firsov, *Science*, 306 (2004) 666.
20. A.K. Geim and K.S. Novoselov, *Nat. Mater*., 6 (2007) 183.

21. V.C. Allen, *Chem. Rev*., 110 (2010) 132.
22. X. Xin, X.F. Zhou, F. Wang, X. Yao, X.X. Xu, Y.M. Zhu and Z.P. Liu, *J. Mater. Chem*., 22 (2012) 7724.
23. S.L. Chou, J.I. Wang, M. Choucair, H.K. Liu, J.A. Stride and S.X. Dou, *Electrochem. Commun*., 12 (2010) 303.
24. J.K. Lee, K.B. Smith, C.M. Hayner and H.H. King, *Chem. Commun*., 46 (2010) 2025.
25. L. Ji, I. Lin, M. Alcoutlabi and X. Zhang, *Energy Environ. Sci*., 4 (2011) 2682.
26. C.K. Chan, H. Peng, G. Liu, K. Mcllurath, X.F. Zhang, R.A. Huggins and Y. Cui, *Nat. Nanotechnol*., 3 (2008) 31.
27. L.M. Li, J. Tang, C.Y. Kang, G.Q. Pan, W.S. Yan, S.Q. Wei and P.S. Xu, *J. Inorg. Mater*., 26 (2011) 472.
28. P.C. Lian, X.F. Zhu, H.F. Xiang, Z. Li, W.S. Yang and H.H. Wang, *Electrochim. Acta*, 56 (2010) 834.
29. M.R. Su, Z.X. Wang, H.J. Gao, X.H. Li, S.L. Huang, W. Xiao and L. Gam, *Electrochim. Acta*, 116 (2014) 230.
30. J.-I. Lee, N.-S. Choi and S. Park, *Energy Environ. Sci*., 5 (2012) 7878.
31. J.K. Feng, Z. Zhang, L.J. Ci, W. Zhai, Q. Ai and S.L. Xiong, *J. Power Sources*, 287 (2015) 177.
32. C.J. Fu, G.G Zhao; H.J. Zhang and S. Li, *Int. J. Electrochem. Sci*., 8 (2013) 6269.
33. J. Guo, A. Sun and C. Wang, *Electrochem. Commun*., 12 (2010) 981.